 doi:10.20944/preprints202210.0188.v1

Article

Focused Analysis of RNFL Decay in Glaucomatous Eyes using Circular Statistics on High-resolution OCT data

Md. Hasnat Ali1,2,3*, Meghana Desai4, S. Rao Jammalamadaka5, Sirisha Senthil1, M. B. Srinivas2,6, Saumyadipta Pyne4,5*

1. L. V. Prasad Eye Institute, Hyderabad, Telangana, India.
2. EEE Department, BITS Pilani Hyderabad Campus, Hyderabad, Telangana, India.
3. Indian Health Outcomes, Public Health and Economics Research (IHOPE) Center, Hyderabad, Telangana, India.
4. Health Analytics Network, Pittsburgh, PA, USA.
5. Department of Statistics and Applied Probability, University of California, Santa Barbara, CA, USA.
6. EEE Department, BITS Pilani Dubai Campus, Dubai, UAE.

* Correspondence: hasali4u@gmail.com, spyne@ucsb.edu

Abstract: Using the OCT platform, we can generate high-resolution data on retinal nerve fiber layer (RNFL) thickness in a given eye at a large number of angular points defined on a circular coordinate system. However, insightful characteristics of OCT RNFL data such as its circularity and granularity generally remain unutilized in its common downstream statistical analyses. We present a new circular statistical framework that defines an Angular Decay function and thereby provides a directional representation of an eye in terms of its focused RNFL loss. By applying to a clinical cohort of Asian Indian eyes, the generated circular data was modeled with a finite mixture of von Mises distributions, which led to unsupervised identification in different age-groups of 2 recurrent clusters of glaucomatous eyes with distinct directional signatures of RNFL decay. New indices of global and local RNFL loss were computed for comparing the structural differences between these glaucoma clusters across the age-groups.

Keywords: Glaucoma; Optical Coherence Tomography; Circular Statistics; Directional Statistics; RNFL; Clustering

Introduction

Progressive optic neuropathies such as glaucoma can cause irreversible blindness, especially when left untreated or diagnosed late. Glaucoma is a chronic ophthalmic disorder characterized by irreversible damage of ganglion cell and retinal nerve fiber layer (RNFL), progressive neuroretinal rim (NRR) thinning, and excavation of the optic nerve head (ONH) (1). It is the second-leading cause of blindness worldwide (2). In 2020, an estimated 80 million individuals worldwide had glaucoma and this number is expected to increase to over 111 million by 2040 (3). In India, the country that is projected to have the largest population by then, more than 16 million could be affected by glaucoma and nearly 1.2 million could be blinded from the disease (4).

Early detection and management hold the key to slowing the progressive loss of vision and preventing blindness due to glaucoma. Yet, a substantial retinal ganglion cell loss could occur before the functional visual field loss from glaucoma is detected (5). In this direction, standard automated perimetry (SAP) has been the gold standard for the detection and management of glaucoma. It provides valuable information about the stage of glaucoma, but not useful for detecting small changes, particularly in early glaucoma. More than 30% of ganglion cell loss is needed before SAP shows the visual field loss (6). However, the platform of spectral-domain optical coherence tomography (SD-OCT) provides excellent glaucoma-diagnostic performance and reproducibility (7,8).

 doi:10.20944/preprints202210.0188.v1

SD-OCT is a non-invasive scanning technology that provides precise, quantitative measurements of the retinal nerve fiver layer (RNFL), optic nerve head (ONH) parameters, neuro-retinal rim (NRR) area, and macular thickness – objective evaluation of these parameters have been used to identify glaucomatous structural damage. As used in the present study, the Cirrus HD-OCT (software version 9.0.0.281; Carl Zeiss Meditec, Dublin, CA, USA) is a computerized instrument that acquires and analyzes cross-sectional and three-dimensional tomograms of the eye. Optic Disc Cube 200x200 protocol is used to scan the ONH and peripapillary area through a 6 mm square grid, which consists of 200 horizontal linear B-scans, and each composed of 200 A-scans.

The most common technique to evaluate RNFL loss from OCT data is peripapillary RNFL measurement based on the calculation circle. Schuman et al. (9) set the scan circle to an arbitrary 3.4 mm diameter (Supplementary Fig. 1a). Subsequently, a 3.46 mm scan circle was set as a standard for glaucoma diagnostic, and all OCT manufacturers adopted the technique. First, the Cirrus HD-OCT algorithm identifies the center of ONH and then automatically places a calculation circle of 3.46 mm diameter evenly around it. Then the system extracts from the data cube 256 A-scan samples and calculates the RNFL thickness at each point along the path of calculation circle. The RNFL measurements along the calculation or scan circle start from the temporal quadrant at 9 o'clock in a clockwise fashion for the right eye and for the left eye at 3 o'clock in a counter-clockwise manner in Temporal-Superior-Nasal-Inferior-Temporal (or TSNIT) order (Supplementary Fig. 1b).

Notably, the above approach makes the OCT platform, along with certain other biomedical scanning technologies, an ideal example of such generators of data that are indexed along multiple well-defined directions – here, at given angular positions equally-spaced around a central point. Unlike the analyses of "linear" data that reside as points on the real line or Euclidean spaces, directional data requires special and altogether different treatment. For instance, a particular direction in two-dimensional plane can be represented as a point on the circumference of a unit circle, or simply as an angle, but neither representation is unique, as both depend on the selection of some appropriate "zero-direction" as the reference starting point of measurement, as well as the sense of rotation, viz., clockwise or anti-clockwise. The unique properties of directional or circular data – for instance, if one wishes to compare or cluster such scans with a suitable distance measure – are appropriately addressed by the fields of directional and circular statistics (10–12).

Traditional OCT analysis often involves a simple division of the circle around ONH into 4 quadrants (of 90 degrees each) or 12 clock-hours (of 30 degrees each) to index and record measurements at these angular sections. Past studies on focused analysis of angular sections of OCT RNFL and NRR data have revealed interesting differences between healthy and glaucoma subjects (13). In this study, we extend such approaches by allowing for analysis of data collected at arbitrarily higher angular resolution that divide the circle (comprising of a total of 360 degrees) into a much larger number (N) of fine sections of 360/N degrees each. While our analytical framework holds in general for any value of N, here, we generated a circular sequence of N=256 data points, which measures RNFL thickness at every 1.41 degrees, for each OCT sample from a human eye. Such high-resolution directional measurements, generated via automated processing of standard SD-OCT images, are ideally suited for application of new and insightful techniques from circular statistics for focused OCT RNFL data, as we introduce in this study.

In addition to age, on the structural side, biological heterogeneity of ONH phenotypes, with or without any neuropathy, can also present challenges to clinical decision-making. Unsupervised learning of the heterogeneity of normative ONH phenotypes in a given population can provide key insights into the diversity of baselines that may exist for degenerative neuropathies, and thus, reduce subjectivity in diagnosis (14). Such knowledge is particularly useful in glaucoma for which different ONH parameters play a combined role in early detection. For instance, in a non-glaucoma multiethnic cohort of Asian individuals, the inter-eye RNFL profile was found by OCT to be less symmetric in

 doi:10.20944/preprints202210.0188.v1

Malays and Indians than that in Chinese eyes (15). Indeed, even the manufacturers of OCT technology noted racial differences in optic disc area, RNFL thickness, etc., when measured using their platform (16).

The present study addresses multiple important aims that include design of an analytical framework that is capable of defining and using a directional measure of RNFL decay based on OCT data and then applying it for focused detection of structural characteristics in glaucomatous eyes from an Indian population. In this direction, our study makes several new contributions. First, we used a large clinical cohort of normal Indian eyes to generate high-resolution OCT RNFL data (as noted above) for each eye. Second, we built a catalog of empirical cumulative distribution functions of RNFL loss at each of the N angular points based on the above data for normal eyes stratified by their age and optic disc size. Third, we developed an analytical framework based on novel applications of circular statistics to OCT data analysis. This includes specifying a directional representation of RNFL decay in a given glaucomatous eye relative to its corresponding normal population. Further, new indices were introduced to measure eye-specific global and local RNFL decay. To illustrate the utility of circular models, we fit a finite mixture of von Mises distributions to identify in glaucomatous eyes two separate clusters of directional representations of RNFL decay. Finally, these clusters, learned in an unsupervised manner for three different age-groups, were characterized using their clinical covariates. In the next section, we describe the Data and Methods, followed by the section on the Results, and end with Discussion.

Data and Methods

Data: All subjects were selected from a population-based study LVPEIGLEAMS (The LV Prasad Eye Institute Glaucoma Epidemiology and Molecular Genetic Study) (17). A total of 3985 healthy eyes of 2225 subjects were included. All subjects were from the rural community of the state of Andhra Pradesh, India. Written informed consent was obtained from all subjects to participate in the study, and the ethics and review committee of the L.V. Prasad Eye Institute reviewed and approved the methodology and was conducted in strict adherence to the tenets of the Declaration of Helsinki. Healthy eyes were defined as in the absence of anterior and posterior pathology.

All participants underwent a comprehensive ophthalmic examination which included a detailed medical and systemic history, best-corrected visual acuity measurement, slit-lamp photographs (Topcon, Bauer Drive, Oakland, NJ), Goldmann applanation tonometry (Hagg-streit AT 900, Hagg-streit AG, Switzerland), gonioscopy with a Sussman four mirror gonioscope (Volk Optical Inc, Mentor, Ohio, USA), dilated fundus examination, central corneal thickness (CCT) assessment, Humphrey visual fields (HVF) with 24-2 Swedish Interactive threshold algorithm (SITA; Carl Zeiss Meditec Inc. Dublin, CA), digital optic disc photography and spectral-domain optical coherence tomography imaging with Cirrus HD-OCT (Carl Zeiss Meditec, Dublin, CA, USA) (18).

Visual fields (VF) were considered if false positive, false negative, and fixation losses less than 20%, and all the stereophotographs of the optic disc had good quality. The inclusion criteria were age ≥ 40 years, best-corrected visual acuity 20/40 or better, spherical equivalent (SE): ± 6D, good quality stereo optic disc photographs, and no media opacities (signal Strength ≥ 6). The exclusion criteria were intraocular surgery within the previous 6 months, any retinal (including macular) or neurologic diseases other than glaucoma that could confound the structural measurements with SD-OCT, RNFL thickness less than 30 μm, and the presence of blink and motion artifacts.

To determine glaucomatous eyes, each digital optic disc photograph was evaluated by three glaucoma specialists independently, and they were masked to the other clinical findings and the other imaging outcomes of the subjects. Each disc photograph was defined as normal based on the absence of superior and inferior NRR thinning, rim notch, disc hemorrhage, and RNFL defect. Eyes were excluded from the study if there were any

Preprints (www.preprints.org) | NOT PEER-REVIEWED | Posted: 13 October 2022 doi:10.20944/preprints202210.0188.v1

discrepancies among the specialists. Finally, from 210 participants, 270 eyes with primary open-angle glaucoma were included in our analysis.

Zeiss' Cirrus HD-OCT software (version 9.0.0.281; Carl Zeiss Meditec, Dublin, CA, USA) uses the segmentation algorithm of the OCT software to identify the RNFL and measures its thickness on the circular peripapillary scan. For each eye (glaucomatous or normal) that was included in our analysis, the same algorithm was used for obtaining its RNFL thickness data at N (=256) equally-spaced (360/N=1.41 degrees apart) angular-points {j:j=1,2,…N} in counterclockwise (TSNIT) direction around the circle (0-360 degrees).

Angular Decay Calculation: The eyes are first stratified according to different combinations of age and disc size. Three age categories (19): Age1 (40-49 years), Age2 (50-59 years), and Age3 (>=60 years), and three optic disc size categories based on OCT disc area measurements: Small (<1.6 mm2), Average (1.6-2.6 mm2), and Large (>2.6 mm2) were used. Thus, by taking all combinations of age and disc size, each eye (normal or otherwise) could belong to exactly one of the 3×3=9 possible groups. For each such group G, and for each angular-point j, we take the set R_(G,j)= {RNFL(i_N,j): normal eye i_N∈G} of RNFL values at the angular point j for every normal eye i_N∈G, and compute the empirical (cumulative) distribution function.

- 〖eCDF〗_(G,j) (x)=|〖r ≤x: r ϵ R〗_(G,j) |/ |R_(G,j) |.

Each function 〖eCDF〗_(G,j) takes as input an RNFL thickness measurement RNFL(i_G,j) of a glaucoma eye i_G∈G at an angular-point j, and returns the corresponding quantile value, which lies in the range [0,1] where 0 and 1 correspond respectively to the lowest and the highest of all RNFL observations at the same angular-point j among the normal eyes that belong to G.

The Angular Quantile of RNFL data for an eye i∈G at an angular-point j is computed as

- Angular Quantile(i,j)= 〖eCDF〗_(G,j) (RNFL(i,j)).

We note that the above quantile value provides a measure that is relative to all the RNFL observations made at a particular angular point over the entire population of normal eyes of the corresponding group. Then the Angular Quantile is computed at each angular point j, which yields for an eye i∈G a circular sequence:

Angular Quantile(i)= {Angular Quantile(i,j):j=1,… N}.

Thus, we define Angular Decay of an eye i∈G as the following circular sequence:

Angular Decay (i)= {1-Angular Quantile(i,j):j=1,…N}.

Hence, for a given eye, at any angular-point, Angular Decay admits a value that lies in the range [0,1]. A higher value of Angular Decay in an eye corresponds to an OCT RNFL measurement that ranks relatively lower among the RNFL observations in the normal population.

Directional representation of RNFL decay: Based on the normal RNFL quantile threshold τ, we characterize the Angular Decay values of a given eye in terms of those that are above versus below τ. Each distinct sequence of contiguous Angular Decay values exceeding τ is defined as a "petal". Therefore, each petal (denoted by Π) represents an angular range that shows higher than normal decay. For a given threshold τ, we denote the number of such petals in an eye by ν_τ. By fixing τ, say, to 0.75, we can drop the suffix in the above quantity (as well as those measurements defined below for each eye) and simply refer to it as ν.

In particular, we are interested in the "widest" petal (π^*) of an eye, which is the largest contiguous sequence of Angular Decay values exceeding τ. We use an algorithm to traverse the circle counter-clockwise and at each successive angular-point j=1, 2…N on the circle of eye i test whether RNFL(i,j) exceeds τ. This yields the starting point (θ_s) and the end point (θ_t) of each existing petal. The counterclockwise circular interval [θ_s, θ_t] defines the angular range of a petal, and the widest petal, i.e., the one with the largest angular range, is identified as π^*.

Preprints (www.preprints.org) | NOT PEER-REVIEWED | Posted: 13 October 2022 doi:10.20944/preprints202210.0188.v1

Since for each angular-point j in the range of π^*, the Angular Decay value is known, we compute the weighted circular mean (20) of π^*where the Angular Decay value at j is used as the weight w_j ϵ [0,1] for the angle θ_j at j. We denote this decay-weighted mean angle (of the largest contiguous region of the eye with above normal Angular Decay) by μ^*, the quadrant specific inverse of the tangent (see Equation 1.3.5 on page 13 of (12))

- μ^*= tan^(-1)⁡〖((∑_(jϵπ^*)▒〖w_j sin⁡〖θ_j 〗〗)/(∑_(jϵπ^*)▒〖w_j cos⁡〖θ_j 〗〗))〗 .

The weighted mean angle allows μ^* to provide a directional representation of an eye in terms of its regional concentration of relatively high RNFL loss. If no such region exists in a given eye for the chosen value of τ, then its μ^* and π^* are denoted by 'NA'.

For unsupervised identification of clusters of eyes in a given collection with distinct directional signatures, the angular data (μ^*) are fitted with a finite mixture of K univariate von Mises distributions ∑_(k=1…K)▒〖α_k vM(μ_k,κ_k)〗 where μ_k and κ_k are respectively the (angular) location and the concentration parameters of the kth component (cluster) of the above mixture whose non-negative proportions {α_k:k=1,…K} add up to 1. The optimal model is selected using the Bayesian Information Criterion (BIC) (21). The absence of at least 2 distinct clusters in a given collection of eyes can be checked for this data with a test of circular unimodality (12). The von Mises distribution vM(μ,κ) has the probability density function (pdf) f(x | μ,κ)=exp⁡〖(κ cos⁡〖(x-μ〗))〗/2πI_0 (κ)〗 , where I_0 (κ) is the modified Bessel function of the first kind of order 0 (12).

Indices of local and global RNFL loss: We define 2 new indices of RNFL loss in a given eye. A measure of local RNFL loss in an eye is defined as the proportion of the size of the angular range of π^* to the entire circle. This local loss index is denoted by λ^*. Further, we also introduce a measure of global RNFL loss in an eye defined by the proportion of the total angular range of all ν petals in this eye to the entire circle. This global loss index is denoted by Λ.

- λ^*= {Number of points j in the angular range of π^* } / N.
- Λ=∑_(Π=Π_1)^(Π_ν)▒{Number of points j in the angular range of Π} / N.

Thus, both measures, λ^*and Λ, take values in the range [0,1], where 0 and 1 represents respectively the minimal and the maximal RNFL loss in a given eye with respect to a chosen threshold τ. We note that 0≤λ^*≤Λ≤1.

Implementation: The above-mentioned framework, including all its functions for analysis and visualization, is implemented using the R platform. The R package movMF was used for fitting a finite mixture of univariate von Mises distributions with EM algorithm to the RNFL decay data represented as a set of angular measurements. For visualization of the Angular Decay in a given eye, we developed a R program that plots this function on a circular scale. Against a background blue circle of radius equal to a selected normal RNFL quantile threshold τ, the Angular Decay function is shown as a circular curve which appears in blue or red when it is below or above τ respectively. Each of the contiguous red sections is a separate petal Π and the widest petal π^* is shown in red.

Results

We generated high-resolution OCT RNFL data with the help of the image processing algorithm of the Cirrus HD-OCT software. Thereby, for each eye, a circular sequence of RNFL thickness data at N=256 equally spaced angular points are obtained for (i) 3985 normal eyes (from 2225 healthy subjects) and (ii) 270 glaucomatous eyes (from 210 subjects) belonging to an Asian Indian cohort. The clinical covariates of the cohort are shown in Table 1. We stratified the cohort in terms of 3 age categories and 3 optic disc size categories (see Methods) into 3×3=9 groups. Thus, for each normal or glaucomatous eye, its group was specified.

Table 1. Clinical covariates of the glaucomatous eyes. (Abbreviations: CD = cup to disc, s.d. = standard deviation, min. = minimum, max. = maximum).

Preprints (www.preprints.org) | NOT PEER-REVIEWED | Posted: 13 October 2022 doi:10.20944/preprints202210.0188.v1

Variable (unit)	mean	median	s.d.	min.	max.
RIM AREA (mm^2)	1.09	1.06	0.25	0.49	1.89
DISC AREA (mm^2)	2.28	2.22	0.59	1.23	4.69
AVERAGE CD RATIO	0.7	0.7	0.1	0.4	0.9
AVERAGE THICKNESS (μm)	86.84	87	9.62	54	112
VERTICAL CD RATIO	0.68	0.69	0.1	0.41	0.88
CUP VOLUME (mm^3)	0.52	0.34	0.49	0.04	3.38
DISK DIAMETER (mm)	1.62	1.6	0.22	1.1	2.4

To determine a statistical reference of the RNFL loss in a glaucomatous eye, we computed (and developed a catalog of) a total of 9×256=2304 direction-specific empirical distribution functions based on RNFL data from the normal eyes that belong to each of the 9 groups (as defined above) and for N=256 angular-points. The process is illustrated with an example in Fig. 1. For a group G of normal eyes, the RNFL thickness circular data are plotted as overlapping curves in Fig. 1(a). In particular, the RNFL measurements of the eyes in G at two particular (but arbitrarily selected) angular points are marked as sets of orange and green points. The empirical distribution functions of these 2 sets are shown as the corresponding orange and green step-functions in Fig. 1(b). Thus, using the cataloged empirical distribution function at each of the angular points (for G), we can compute the normal RNFL thickness range for any given quantile (or equivalently, percentile). In Fig. 1(c), for selected quantile values (the 5th, 25th, 50th, and 75th percentiles), the increasing ranges of RNFL thickness are shown as successive contour curves (in red, yellow, orange, and green respectively). If the RNFL circular data of any new eye i is overlaid on this contour plot, it will reveal the precise extent of any overall or focused RNFL loss relative to the normal RNFL circular distribution of the group that i belongs to.

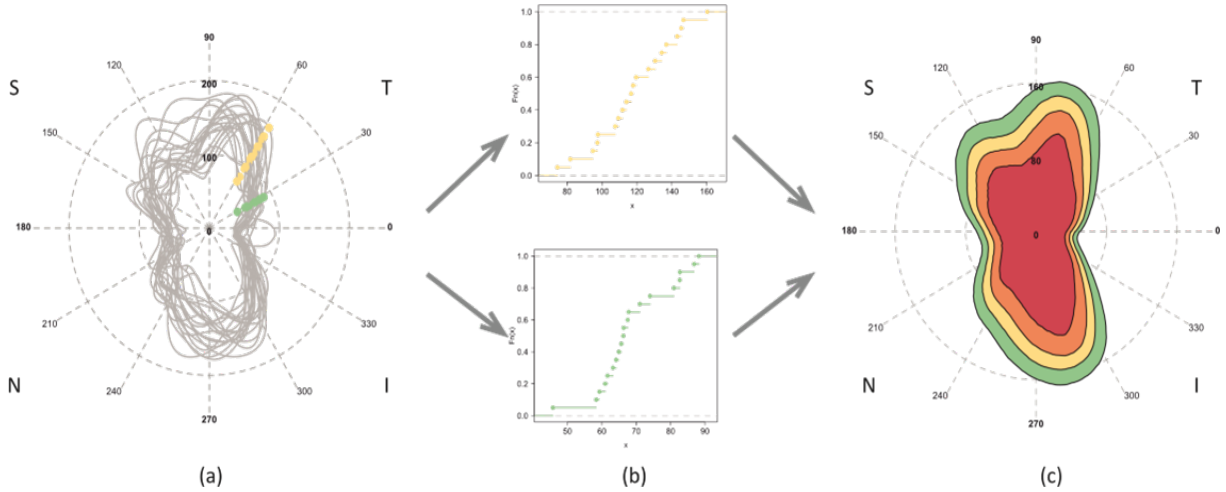

Figure 1. The circular OCT RNFL thickness data for normal eyes belonging to a group are overlaid and shown in plot (a). Two examples of angular points are used to mark the OCT data as sets of green and orange points. Plot (b) shows the eCDF functions for these two OCT datasets. Plot (c) shows the ranges of normal RNFL thickness values for different Angular Quantiles. As examples, the concentric ranges for the 5th, 25th, 50th, and 75th percentiles are shown with red, orange, yellow, and green contours respectively.

Preprints (www.preprints.org) | NOT PEER-REVIEWED | Posted: 13 October 2022 doi:10.20944/preprints202210.0188.v1

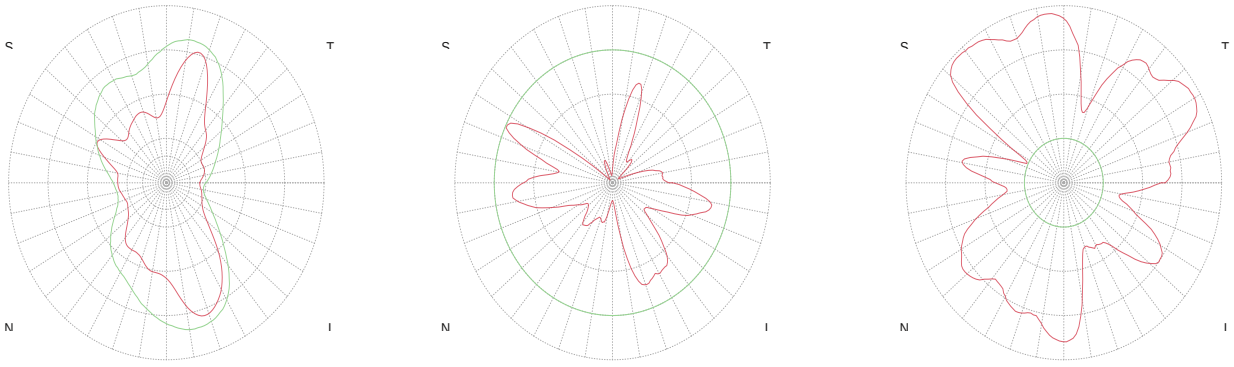

(a) (b) (c)

Figure 2. The circular OCT RNFL thickness data of a glaucomatous eye is shown as a red curve in plot (a). For reference, the 75th percentile of normal RNFL thickness is shown with a green curve. The glaucomatous and normal RNFL data are converted to their respective Angular Quantiles (of range [0,1]) and shown as the corresponding red and green curves in plot (b). In (c), the complementary plot of (b) shows the RNFL Angular Decay (of range [0,1]) as red and green curves for the glaucomatous and normal cases respectively.

Preprints (www.preprints.org) | NOT PEER-REVIEWED | Posted: 13 October 2022 doi:10.20944/preprints202210.0188.v1

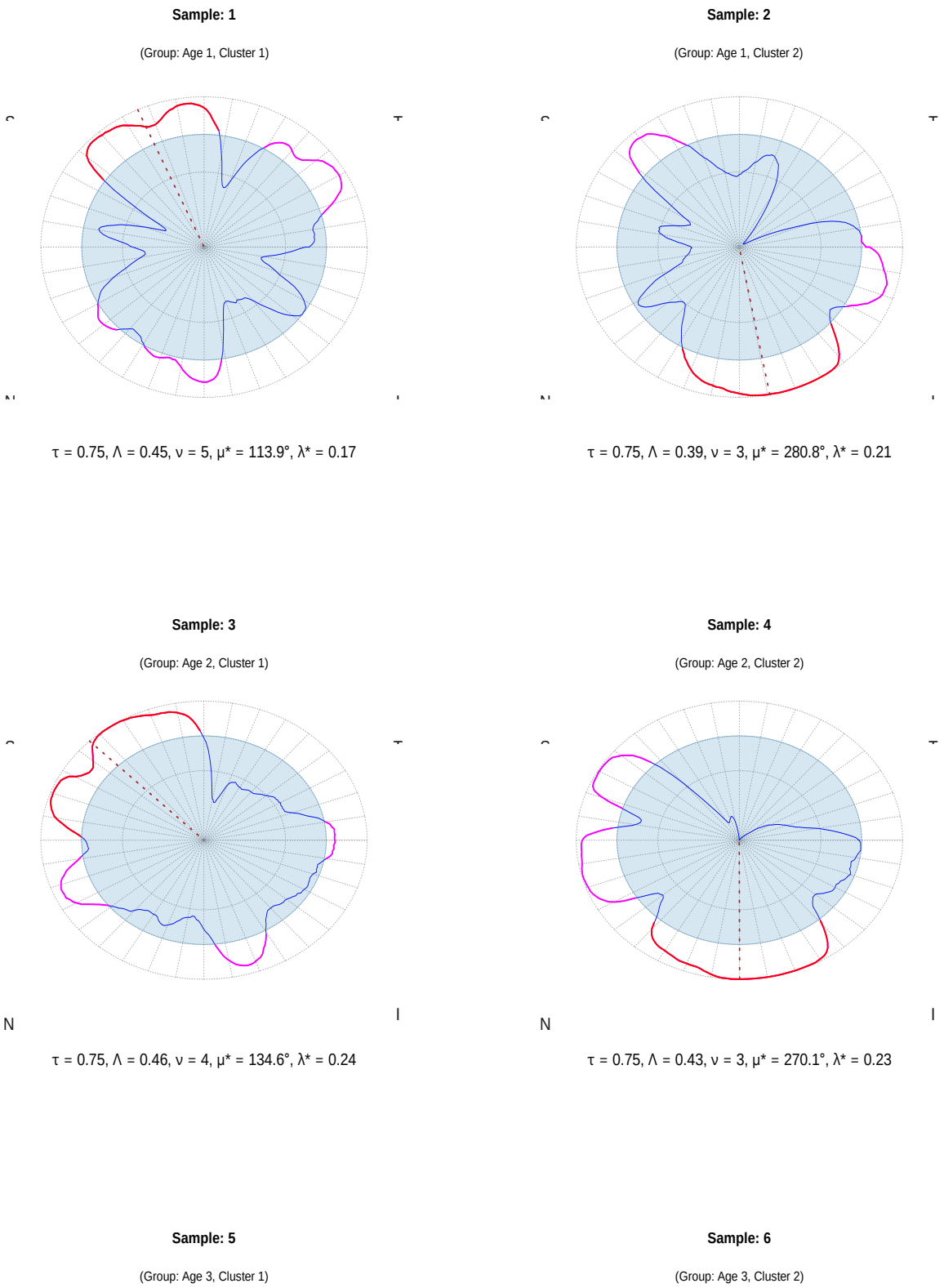

Figure 3. For 6 samples of glaucomatous eyes, the RNFL Angular Decay functions are plotted. Each plot contains a pale blue circle of radius equal to the threshold of decay ◎ set at 0.75. The petals lying above the pale blue circle are shown as pink curves. The petal with the largest angular range is marked with a red curve. The weighted circular mean angle of the red petal is shown with a dashed red line. Various indices computed for each eye are shown below the plot of each sample.

Preprints (www.preprints.org) | NOT PEER-REVIEWED | Posted: 13 October 2022 doi:10.20944/preprints202210.0188.v1

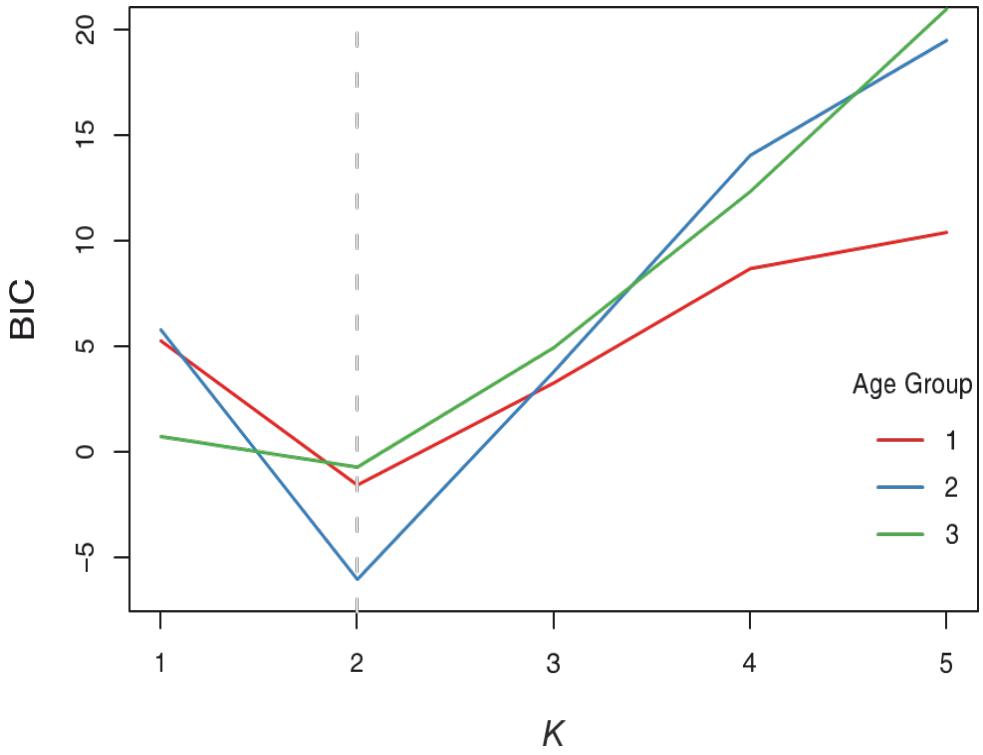

Figure 4. The BIC values corresponding to different choices of the number of components, K, in the mixture model of von Mises distributions fitted to circular data from 3 age-groups.

Preprints (www.preprints.org) | NOT PEER-REVIEWED | Posted: 13 October 2022 doi:10.20944/preprints202210.0188.v1

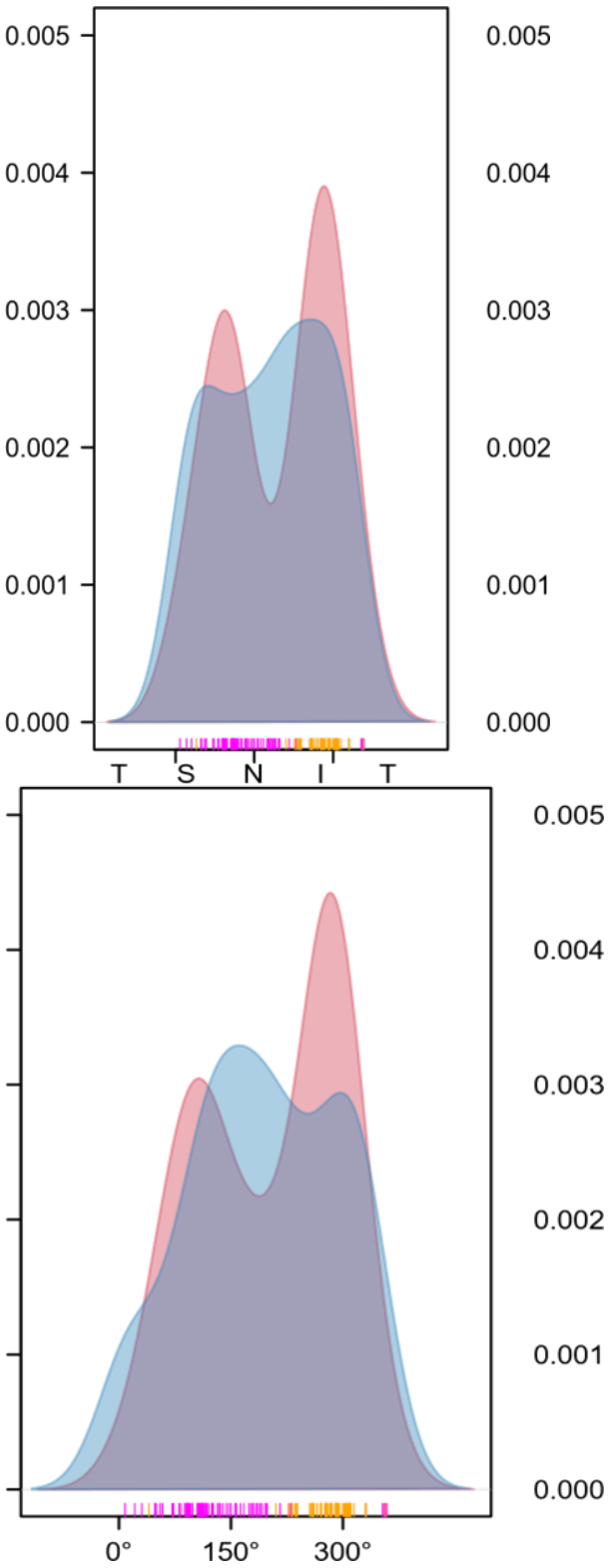

Preprints (www.preprints.org) | NOT PEER-REVIEWED | Posted: 13 October 2022 doi:10.20944/preprints202210.0188.v1

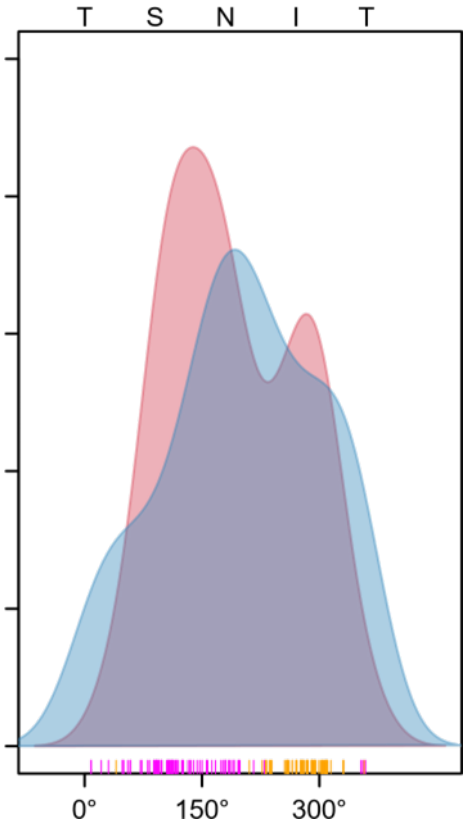

Figure 5. The distributions of circular data based on the angular representation of glaucomatous eyes from 3 age-groups are shown as red histograms in plots (a), (b) and (c). The corresponding normal distributions are shown as blue histograms. The assignment of the eyes to 2 clusters by the mixture model is shown as pink and orange points in the rugplot below the histograms. The TSNIT order of the circular range (0-360 degrees) is shown above the plots.

An innovative feature of the present study is its method of calculating Angular Decay measure as a circular function based on an eye i's high-resolution OCT RNFL data. It begins with RNFL thickness data of i at a particular angular-point j. Given the group G that i belongs to, and j, the corresponding empirical distribution function (as described above) is used as the relevant reference of normal RNFL thickness for calculating the precise quantile value of the focused RNFL data. This is shown as the red curve in Fig. 2(a) whereas the green curve, which represents the 75th percentile (or the quantile of 0.75) of the normal RNFL distribution, serves as a reference. We transform the RNFL data into their respective Angular Quantiles and plot these as the corresponding red and green curves in Fig. 2(b). The exact complementary plot of Fig. 2(b), computed as {1-Angular Quantiles ()}, produces the Angular Decay function that is shown by the analogous red and green curves in Fig. 2(c).

By taking an arbitrary (but real) eye as an example, its RNFL data and the corresponding Angular Quantile and Angular Decay functions are shown as red curves in Fig. 2(a), 2(b) and 2(c) respectively. As noted above, for comparison, the 75th percentile values of the corresponding normal RNFL distribution are also marked in the same plots as green curves. Interestingly, the Angular Decay function at each point of the circle relative to the normal threshold (τ=0.75) as shown in Fig. 2(c) provides a more noticeable and focused visualization of the overall phenomenon of RNFL loss as compared to the other plots, viz., Fig. 2(a) and 2(b). To gain further insights, our framework allows altered settings of the normal quantile threshold (τ) that enable the user to identify subtle local dynamics of RNFL decay as well as conduct comparative analysis, say, across eyes from different groups and time-points.

 doi:10.20944/preprints202210.0188.v1

The more noticeable and distinctive features of an Angular Decay plot is due to the underlying Decay function that highlights the contiguous regions of RNFL loss. We identified these regions with a circular tracing algorithm which uses a user-defined quantile threshold (τ) to demarcate the "petals" which are contiguous regions with Decay exceeding τ. Furthermore, we compute insightful characteristics of the petals, and thereby distinguish the patterns of RNFL Decay in the eye under consideration, using 4 new indices, which we illustrate using real data in Fig. 3. The Angular Decay functions of 6 glaucomatous eyes are shown in Fig. 3 as examples of our graphical output. For each eye, the selected quantile threshold is shown as a pale blue circle of radius τ. The Decay function is shown as blue or pink curves depending on whether it is below or above τ. Each contiguous pink angular segment represents a separate petal (Π). In a given eye, for fixed τ, the total number of petals is denoted by ν; and the petal with the largest angular range is depicted as a red curve and denoted by π^*.

The systematic identification of π^* allows us to define an angular representation of an eye in terms of its largest contiguous segment of above normal RNFL decay. For this purpose, we compute the weighted circular mean of π^*, which is, conceptually, the angle (denoted by μ^*) around which the RNFL decay within the widest petal of the eye is concentrated. The weighting used in the calculation of μ^* captures the contribution of the variations of the shape of π^*, which results in a more precise directional representation of the decay. The angular value of μ^* for each eye is shown as a dashed red line in the Angular Decay plots of Fig. 3.

In addition to capturing the directional information, we are also interested to quantify the proportion of decay that is described by π^* as it represents the widest petal of an eye. Thus, we define a measure of local loss of RNFL of an eye, denoted by λ^*, as the fraction of the circle (of total 360 degrees) that is covered by the angular segment corresponding to π^*. Further, we introduce another index for measuring the global loss of RNFL for an eye, denoted by Λ, as the fraction of the circle (of total 360 degrees) that is covered by the union of the angular segments corresponding to all the petals in an eye. Here, it may be noted that both the above indices of RNFL loss are determined upon fixing a quantile threshold (τ) on the corresponding normal RNFL distribution. In Fig. 3, below each eye's Angular Decay plot, the computed values of its different indices are shown.

The new measures could be used singly or in combination for downstream analysis of OCT data such as quantitative comparison of samples or mining for various patterns of RNFL decay. To demonstrate such uses of circular data in OCT analysis, we applied finite mixture modeling, a popular technique for unsupervised learning of groups or clusters in a given collection of samples (here, glaucomatous eyes). In particular, we fitted a finite mixture of univariate von Mises or "circular normal" distributions separately to 3 directional datasets on μ^* values of glaucomatous eyes. First, we partitioned the glaucomatous eyes in the cohort into 3 age-groups: Age1 (40-49 years), Age2 (50-59 years), and Age3 (>=60 years). Then, each group's dataset on μ^* was modeled with a mixture of G (=1, 2…5) von Mises distributions with the aim of checking whether there are different clusters of glaucomatous eyes in these age-groups. Here, G=1 implies a unimodal distribution of data that does not multiple distinct clusters. The models were fitted using the EM algorithm and the optimal model was selected based on the value of G for which BIC is the minimum (Fig. 4).

Interestingly, the optimally fitted circular normal mixture models identified 2 clusters (representing G=2 mixture components) of glaucomatous eyes – in all 3 age-groups – with very distinct directional patterns of RNFL decay (red histograms in Fig. 3). The estimated parameters of the selected models are shown in Table 2. In particular, we note that the 2 clusters align clearly across the 3 age-groups in terms of their very distinct estimates of the angular location parameter (μ) of the von Mises distribution that was fitted for identifying each component of the mixture. Relative to the higher RNFL thickness of the normal eyes in the Superior (S) and Inferior (I) sectors (see the green distribution in Supple-

Preprints (www.preprints.org) | NOT PEER-REVIEWED | Posted: 13 October 2022 doi:10.20944/preprints202210.0188.v1

mentary Fig. 1(b)), the decay in the glaucomatous eyes is concentrated around these regions (the red "modes" in Fig. 5) for all 3 age-groups. The rugplot at the bottom of the red histograms in Fig. 5 depicts the membership of the glaucomatous eyes into these 2 clusters – using pink and orange points – as assigned by the fitted mixture model. In clear contrast to the glaucomatous eyes, the distributions of angular representation of RNFL data from the normal eyes of the same age groups appear much less distinctly multimodal in the blue histograms in Fig. 5.

Table 2. The estimates of the parameters of a 2-component mixture model of von Mises distributions for 3 age-groups. The Bayesian Information Criterion (BIC) value for each optimal model is shown.

Group	Component	μ (degrees)	κ	α	BIC
Age1	Cluster1	101.97	11.044	0.304	-1.506
	Cluster2	296.26	1.556	0.696	
Age2	Cluster1	120.01	0.882	0.616	-6.015
	Cluster2	286.48	13.833	0.384	
Age3	Cluster1	146.45	1.247	0.784	-0.665
	Cluster2	291.77	14.932	0.216	

Table 3. The mean values of the clinical covariates of the glaucomatous eyes belonging to the 2 identified clusters in 3 age-groups. (Abbreviation: CD = cup to disc).

	Cluster1			Cluster2		
Variable (unit)	Age1	Age2	Age3	Age1	Age2	Age3
RIM AREA (mm^2)	1.09	1.09	1.13	1.02	1.09	1.05
DISC AREA (mm^2)	2.36	2.47	2.2	2.2	2.23	2.14
AVERAGE CD RATIO	0.72	0.72	0.68	0.7	0.68	0.7
AVERAGE THICKNESS (μm)	87.65	89.57	86.96	87.42	85.29	83.16
VERTICAL CD RATIO	0.68	0.69	0.66	0.69	0.69	0.69
CUP VOLUME (mm^3)	0.57	0.66	0.4	0.62	0.51	0.36
DISK DIAMETER (mm)	1.64	1.7	1.59	1.59	1.58	1.57

For further characterization of the 2 clusters of glaucomatous eyes identified in different age-groups solely by their angular representation of RNFL decay, we studied their clinical covariates. In Table 3, we note that many of the clinical covariates of the glaucomatous eyes that belong to these 2 clusters have distinctive mean values. A visual comparison of such covariates across the 2 clusters in the 3 age-groups is shown in the boxplots of Supplementary Fig. 2. For consistency, we used the same pink and orange color scheme for the corresponding clusters as in Fig. 5. Further, when we compared the values of the new indices of global (Λ) and local loss (λ^*) of RNFL, we again observed clear differences in the structural changes across the same clusters in different age-groups. Intriguingly, whereas the covariates and the global loss index could distinguish between the clusters in the glaucomatous eyes of the two younger groups, for the oldest group (Age3: ≥ 60 years), the distinction is pronounced only when we compared their indices of local RNFL loss λ^*. We note that λ^* clearly admits of higher values for the eyes in cluster 2 than those in cluster 1, which further underscores the utility of directional or focused analysis of OCT data.

Discussion

The OCT platform has the ability to produce reproducible scans of an eye that could be read out as a high-resolution sequence of measurements made at a fairly large number (N=256 in the present study) of evenly spaced angular points defined on a circular coordinate system. However, both of these insightful characteristics of OCT data – its granularity (N) and circularity – generally remain unutilized in its usual downstream statistical analyses. Indeed, clinical applications may use results that are summarized over a much

 doi:10.20944/preprints202210.0188.v1

smaller number of angular segments, e.g., 4 quadrants or 12 clock-hours, and then too, the RNFL values therein are treated not in terms of their directionality but only in terms of their magnitude. Hence, any comparison of OCT RNFL data, as is often done for patient classification or comparing across time-points, is generally restricted to the linear scale.

In the present study, we present a new circular statistical framework that used both the directionality as well as the magnitude of readily available OCT RNFL data. This framework could be straightforwardly generalized, and applied, to other comparable types of data, such as OCT NRR, Fundus imaging, etc. In addition, we generate new high-resolution SD-OCT data to compute focused Angular Decay Functions. These mathematical functions provide a quantitative measure of RNFL loss relative to the normal population at every 1.41 degree in a common circular coordinate system. Moreover, we provide an algorithm to identify the petals or contiguous regions, defined as precisely specified angular intervals, at which the RNFL decay in a given eye exceeds a threshold that is specified with an intuitive quantile (or percentile) of the corresponding normal RNFL empirical distribution.

Importantly, based on the above framework, we introduced two measures of local and global RNFL decay in a given eye relative to that in the normal eyes. In fact, we combined both the directionality (denoted by an angle) and the magnitude (by a weight) of the OCT data to define a new quantitative but angular representation of a given eye's RNFL decay. The new representation opens up the potential for creative applications of the rich variety of tests and tools that exist in the fields of directional and circular statistics for insightful OCT data analysis. We demonstrated this by fitting a mixture of von Mises (also known as "circular normal") distributions to the directional data generated in the present study, which led to unsupervised identification of 2 clusters with distinctive focused patterns of RNFL decay in 3 different age groups of a cohort of glaucomatous eyes from the Indian population. Moreover, the new indices of global and local RNFL loss were effective in capturing the structural differences between these glaucoma clusters.

We emphasize that, to accurately account for the effects of normal variation in RNFL, ideally, normative databases of healthy eye OCT phenotypes that are large and racially representative should be developed. However, often such collections of healthy samples tend to be small or moderately sized, e.g., the normative database of Cirrus HD-OCT platform included just 284 subjects of which the representation of Indians is about 1% (16). Clearly, this does not adequately reflect the 2020 projections about India which is to become the second in global glaucoma numbers, surpassing Europe (4). In this direction, our rigorous cataloging of the more than 2300 empirical distribution functions of RNFL thickness, which takes into account the variations of age and optic disc sizes in the normal population, not only provides a quantitative reference for the focused angle-specific decay in the glaucomatous eyes but also addresses the disparity in the form of under-representation of Indian phenotypes in the common normative OCT databases.

We understand that there are certain limitations of the study. While our adaptation of the image processing algorithm, as implemented in the standard Cirrus HD-OCT software package, for generating the N=256-point circular RNFL data is straightforward, we understand that such high-resolution data extraction is not common in OCT analysis. Moreover, the focused and angular measure of the new directional representation of RNFL loss renders it difficult to conduct a direct comparison with any traditional indices that are based on the magnitude (but not directionality) of such decay. Finally, we identified, in 3 different age-groups, 2 recurrent clusters of glaucomatous eyes with very distinct directional signatures of RNFL decay. In future work, we will provide further characterization of the clusters with more rigorous investigation that goes beyond the scope of the present study.

While past studies have used spatial, trigonometric and Fourier analysis on OCT data, e.g., (22–25), our framework, involving directional or circular data, is methodologically quite different from those approaches. While our earlier platform CIFU (14) focuses on the aspects of shapes and curves in OCT NRR data, as in functional data analysis

 doi:10.20944/preprints202210.0188.v1

(FDA), it does not explicitly address the directional characteristics of OCT data or angular measurements thereof. We have demonstrated the utility of both the granularity and the directionality of OCT data and combined these with an angle-based description of patterns that could be studied with innovative downstream analyses. Indeed, processes or platforms that generate data which are capable of being represented as angular values (e.g., wind direction, neuronal activity) require altogether different statistical approaches as compared to usual linear data (10). We think that the new directional representation of OCT data to capture an eye's RNFL decay will pave the way for future applications of the rich methodology of directional and circular statistics (10–12) to eye data analysis.

Author Contributions:S.P. conceived and designed the study. M.H.A., S.R.J., M.D., M.B.S., and S.P. planned the steps for analysis. M.H.A. and S.S. collected the data. M.H.A. and S.P. analyzed the data. All authors contributed to the writing of this manuscript.

Conflicts of Interest: The authors declare no conflict of interest.

Funding: This study received no external funding.

References

1. Chrysostomos D, Dimitriou DCB. Pathophysiology of glaucoma. In: Ichhpujani P, editor. Glaucoma: Basic and Clinical Perspectives. 2013. p. 32–57.
2. Global initiative for the elimination of avoidable blindness: action plan 2006-2011 [Internet]. World Health Organization. 2007. Available from: https://apps.who.int/iris/handle/10665/43754
3. Tham Y-C, Li X, Wong T, Quigley H, Aung T, Cheng C-Y. Global prevalence of glaucoma and projections of glaucoma burden through 2040: a systematic review and meta-analysis. Ophthalmology. 2014; 121:2081–90.
4. Quigley H, Broman AT. The number of people with glaucoma worldwide in 2010 and 2020 [Internet]. British Journal of Ophthalmology Mar 1, 2006, p. 262–7. Available from: https://pubmed.ncbi.nlm.nih.gov/16488940/
5. Quigley HA, Addicks EM, Green RW, Green WR. Optic Nerve Damage in Human Glaucoma: Iii. Quantitative Correlation of Nerve Fiber Loss and Visual Field Defect in Glaucoma, Ischemic Neuropathy, Papilledema, and Toxic Neuropathy. Arch Ophthalmol [Internet]. 1982 Jan 1 [cited 2021 Jan 23];100(1):135–46. Available from: https://pubmed.ncbi.nlm.nih.gov/7055464/
6. Kerrigan–Baumrind LA, Quigley HA, Pease ME, Kerrigan DF, Mitchell RS. Number of Ganglion Cells in Glaucoma Eyes Compared with Threshold Visual Field Tests in the Same Persons. Investig Ophthalmol Vis Sci. 2000; 41:741–8.
7. Leung CKSS, Lam S, Weinreb RN, Liu S, Ye C, Liu L, et al. Retinal nerve fiber layer imaging with spectral-domain optical coherence tomography: analysis of the retinal nerve fiber layer map for glaucoma detection. Ophthalmology [Internet]. 2010 Dec 1 [cited 2022 Sep 16];117(9):1684–91. Available from: https://pubmed.ncbi.nlm.nih.gov/20678802/
8. Leung CK shun, Cheung CY lui, Weinreb RN, Qiu Q, Liu S, Li H, et al. Retinal Nerve Fiber Layer Imaging with Spectral-Domain Optical Coherence Tomography. A Variability and Diagnostic Performance Study. Ophthalmology [Internet]. 2009 Jul 1 [cited 2022 Sep 16];116(7):1257-1263.e2. Available from: http://www.aaojournal.org/article/S0161642009003650/fulltext
9. Schuman JS, Pedut-Kloizman T, Hertzmark E, Hee MR, Wilkins JR, Coker JG, et al. Reproducibility of Nerve Fiber Layer Thickness Measurements Using Optical Coherence Tomography. Ophthalmology [Internet]. 1996 Nov 1 [cited 2022 Sep 16];103(11):1889. Available from: /pmc/articles/PMC1939724/
10. Cremers J, Klugkist I. One direction? A tutorial for circular data analysis using R with examples in cognitive psychology. Front. Psychol. 2018 Oct 30;9(OCT):2040.
11. Mardia K V., Jupp PE. Directional Statistics. Wiley Series in Probability and Statistics. 1999.
12. Jammalamadaka S Rao, SenGupta A. Topics in Circular Statistics. World Scientific Publishing Co., 2001.
13. Hwang YH, Kim YY. Glaucoma Diagnostic Ability of Quadrant and Clock-Hour Neuroretinal Rim Assessment Using Cirrus HD Optical Coherence Tomography. Invest Ophthalmol Vis Sci. 2012 Apr 1;53(4):2226–34.
14. Ali MH, Wainwright B, Petersen A, Jonnadula GB, Desai M, Rao HL, et al. Circular functional analysis of OCT data for precise identification of structural phenotypes in the eye. Sci Reports 2021 111 [Internet]. 2021 Dec 2 [cited 2022 Sep 16];11(1):1–13. Available from: https://www.nature.com/articles/s41598-021-02025-4
15. Tao Y, Tham YC, Chee ML, Majithia S, Thakur S, Soh Z Da, et al. Profile of retinal nerve fibre layer symmetry in a multiethnic Asian population: The Singapore Epidemiology of Eye Diseases study. Br J Ophthalmol. 2020; 104:836–41.
16. Knight OJ, Girkin CA, Budenz DL, Durbin MK, Feuer WJ. Effect of race, age, and axial length on optic nerve head parameters and retinal nerve fiber layer thickness measured by cirrus HD-OCT. Arch Ophthalmol. 2012;130(3):312–8.
17. Addepalli UK, Jonnadula GB, Garudadri CS, Rao HL, Rani PK, Chakrabarti S, et al. LV Prasad Eye Institute Glaucoma Epidemiology and Molecular Genetic Study (LVPEI- GLEAMS). Report 1: study design and research methodology. Ophthalmic Epidemiol [Internet]. 2013 Jun [cited 2022 Sep 16];20(3):188–95. Available from: https://www.tandfonline.com/doi/abs/10.3109/09286586.2013.792938

18. Carl Zeiss Meditec Inc. Cirrus HD-OCT User Manual (Carl Zeiss Meditec Inc, 2015).
19. Rao HBL, Sekhar GC, Babu GJ, Parikh RS. Clinical measurement and categorization of optic disc in glaucoma patients. Indian J Ophthalmol [Internet]. 2009 Sep 1 [cited 2022 Sep 16];57(5):361. Available from: /pmc/articles/PMC2804124/
20. Basu S, Jammalamadaka RS. Unimodality in Circular Data: A Bayes Test. In: Balakrishnan; N., editor. Advances on Methodological and Applied Aspects of Probability and Statistics [Internet]. 1st ed. CRC Press; 2020. p. 141–58. Available from: https://www.taylorfrancis.com/chapters/edit/10.1201/9780203493212-8/unimodality-circular-data-bayes-test-sanjib-basu-rao-jammalamadaka
21. Schwarz G. Estimating the Dimension of a Model. Ann Stat [Internet]. 1978 Mar 1 [cited 2021 Jul 16];6(2):461–4. Available from: https://projecteuclid.org/journals/annals-of-statistics/volume-6/issue-2/Estimating-the-Dimension-of-a-Model/10.1214/aos/1176344136.full
22. Zhu W, Kolamunnage-Dona R, Zheng Y, Harding S, Czanner G. Spatial and spatio-temporal statistical analyses of retinal images: a review of methods and applications. BMJ Open Ophthalmol [Internet]. 2020 May 1 [cited 2022 Sep 17];5(1):e000479. Available from: https://bmjophth.bmj.com/content/5/1/e000479
23. Pyne S, Ali MH, Aruru M, Rao HL. Quantification of retinal nerve fiber layer changes in optical coherence tomography images reveals differential progression of glaucomas. BLDE Univ J Heal Sci [Internet]. 2019 [cited 2022 Sep 17];4(2):85. Available from: https://www.bldeujournalhs.in/article.asp?issn=2468-838X;year=2019;volume=4;issue=2;spage=85;epage=89;aulast=Pyne
24. Essock EA, Sinai MJ, Bowd C, Zangwill LM, Weinreb RN. Fourier Analysis of Optical Coherence Tomography and Scanning Laser Polarimetry Retinal Nerve Fiber Layer Measurements in the Diagnosis of Glaucoma. Arch Ophthalmol [Internet]. 2003 Sep 1 [cited 2022 Sep 17];121(9):1238–45. Available from: https://jamanetwork.com/journals/jamaophthalmology/fullarticle/415637
25. Hsieh MH, Chang YF, Liu CJL, Ko YC. Fourier analysis of circumpapillary retinal nerve fiber layer thickness in optical coherence tomography for differentiating myopia and glaucoma. Sci Reports 2020 101 [Internet]. 2020 Jun 29 [cited 2022 Sep 17];10(1):1–9. Available from: https://www.nature.com/articles/s41598-020-67334-6